Hidden features in (Bi,Pb)-2223 granular superconductors

M. Hernández-Wolpez
Departamento de Física Universidad de Camagüey,
Ctra. Circunvalación Norte, Km 5 1/2, Camagüey, Cuba.
e-mail: manuel.hwolpes@reduc.edu.cu

E. Martínez-Guerra
Centro de Investigación en Materiales Avanzados S.C., Unidad Monterrey-PIIT,
Apodaca, Nuevo León 66600, México.

R.F. Jardim
Instituto de Física, Universidade de São Paulo,
CP 66318, 05315-970, S. Paulo, SP, Brazil.

P. Muné
Departamento de Física, Universidad de Oriente,
Patricio Lummumba s/n, P. O. Box 90500, Santiago de Cuba, Cuba.

Received 9 October 2015; accepted 17 June 2016

The aim of this review is to give a summary of some hidden features related to penetration, trapping, and relaxation of the magnetic flux in (Bi,Pb)-2223 granular superconductors. The discussion is based on experimental and theoretical results obtained in samples prepared under different conditions and by different research groups. Fundamental concepts such as granularity and grain boundaries **(GB)**, superconducting levels, types of vortices, and microstructural characteristics of (Bi,Pb)-Sr-Ca-Cu-O superconductors are invoked for supporting the discussion. As conclusions we focus on the main insufficiencies in the treatment and understanding of the phenomena mentioned above. We also propose some experiments for improving the understanding of the general physical features of granular superconductors.

Keywords: (Bi; Pb)-2223 superconductors; superconducting levels; magnetic flux-trapped; nanometer Al_2O_3 addition; microstructure.

PACS: 74.72.Hs; 74.25.Wx; 74.62.Dh; 74.62.Bf.

1. Introduction

Since the discovery of high-T_c superconductors **(HTS)** [1] the study of phenomena such as penetration, trapping and relaxation of magnetic flux has been an important task to the understanding of the main properties of these materials. Among cuprate high-T_c superconductors, Bi-2223 [2] is one of the most studied due to its very large potential for practical applications [3]. Some authors have determined the lower critical field, H_{c1} [4–9] that represents the field intensity at which is thermodynamically allowed the penetration of magnetic flux within the superconductor [10]. However, the external magnetic field at which the penetration is first observed depends, at least, of three aspects as (i) the specific region of the material where the penetration first occurs; (ii) the demagnetizing factor of the sample; and (iii) the anisotropy of the superconducting material, the latter being very high in Bi-2223 superconductors. Due to these aspects, different values of H_{c1} have been reported in different specimens of Bi-2223 superconducting materials such as thin films, whiskers, and ceramics, and a detailed and consistent discussion on this wide spectrum of different values is absent in the literature. A precise determination of H_{c1} is also difficult when polycrystalline samples are considered due to the presence of pores, cracks, **GB**, and extra-phases [11] that certainly alter the measurement of H_{c1}.

Nowadays, in order to improve the magnetic flux pinning of the materials, artificial flux pinning centers are introduced by using two main procedures: irradiation with high energy ions [12–17] and by addition of inorganic nanoparticles [18–25]. Several works have reported the effects of the addition of nanoparticles of $\alpha-Al_2O_3$ (Bi,Pb)-2223 ceramics [23–25] but such effects in the trapping of inter and intragranular vortices has not been discussed in details.

Finally, the relaxation of the magnetic flux trapped inside the superconducting materials has been also studied theoretically and experimentally due to its importance for practical applications. The difficult here is not related directly to the electrical resistivity of the material but by the motion of thermally activated vortices inside the superconductor [26]. As far as this point is concerned, E. Altshuler *et al*. [27] have reported the voltage relaxation in polycrystalline samples of $YBa_2Cu_3O_{7-x}$. The experimental study was carried out by means of transport measurements and the voltage detected by the four probe method was taken as an indirect measurement of the intragranular magnetization, as reported by D.N. Matthews *et al*. and R. Decca *et al*. [28, 29]. However, for samples subjected to an applied magnetic field lower than the critical field of the grains no relaxation has been observed. The authors have then concluded that their samples did not exhibit any trapped flux in the intergranular region, at least in the limit of the experimental detection [27].

Based on the described above, the goal of this review is to guide the reader in the direction of both experimental and theoretical results related to the penetration, trapping, and relaxation of the magnetic flux in (Bi,Pb)-2223 polycrystalline superconductor showing incomplete results that can be improved and refined in the light of the new results obtained in bicrystals and thin films. To achieve this objective, the paper has been organized in the following form. The next section (Sec. 2) treats of some concepts and main ideas such as granularity and **GB**, superconducting levels, types of vortices, and some microstructural characteristic of (Bi,Pb)-2223 superconductors. The theoretical and experimental results related to the penetration, trapping and relaxation of the magnetic flux appear in Sec. 3, where every phenomenon is analyzed independently. Finally, Sec. 4 presents the conclusions and the proposition of new experiments and studies to improve the understanding of these phenomena in (Bi,Pb)-2223 materials.

2. Main concepts

2.1. Granularity and grain boundaries

The presence of microscopic heterogeneities and certain intrinsic properties of **HTS** are responsible for a very important characteristic of polycrystalline materials: the so-called granularity. Granularity may be understood as the coexistence in the same material of several superconducting levels which are characterized by different critical parameters. In a first approach, two different superconducting levels may be distinguished in a polycrystalline **HTS**: (1) intragranular (or strong level); and (2) intergranular (or weak level) [30]. Thus, the superconducting behavior of the grains in the presence of a thermodynamic parameter as applied magnetic field, for instance, exhibits a higher response, which is corroborated by the high values of their superconducting critical parameters when compared with those observed in the intergranular region where such critical parameters are reduced appreciably [31]. This granularity, always present in **HTS**, limits strongly the electrical transport current that can flow through the superconducting material without losses and restricts their technological applications [31].

The electrical resistance of a **HTS**, which carries an electrical current and it is subjected to an applied magnetic field, depends on the angle between the applied magnetic field and the current density. In a single crystal specimen, such an angle corresponds to that between the magnetic field and the current density while in the polycrystalline sample is necessary to take into consideration the random orientation of the grains, their anisotropy and intrinsic granularity [32], since the granualrity is also observed in the case of single crystal induced by its high anisotropy. The anisotropy of the physical properties of (Bi,Pb)-2223 superconductors, is also commonly observed in highly textured materials as sheathed tapes with silver, where the ratio of the current densities between the main directions at low temperature is $J^{ab}/J^{c} \approx$ [33].

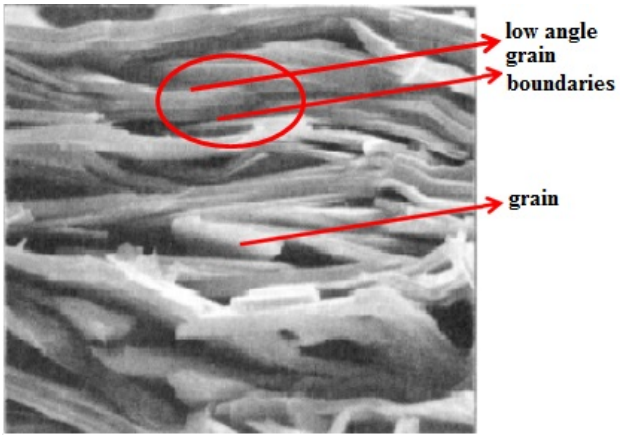

FIGURE 1. SEM image of the transverse fracture surface of a (Bi,Pb)-2223 filament with J_c (77 K, 0 T) = 2.5×10^4 A/cm^2 (Figure modified from H. Hilgenkamp and J. Mannhart [34]).

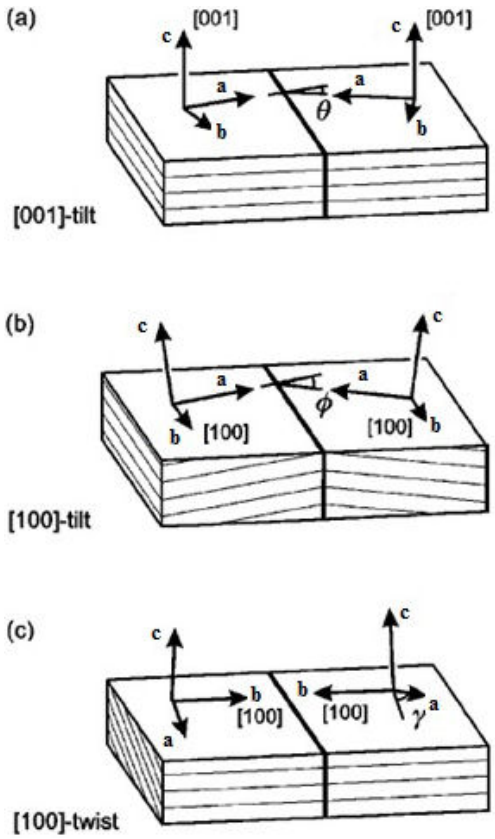

FIGURE 2. Schematic diagram showing the crystallography of **(a)** a [001]-tilt boundary, **(b)** a [100]-tilt boundary, and **(c)** a [100]-twist boundary in a cubic material. (Figure modified from H. Hilgenkamp and J. Mannhart [34]).

One of the characteristics of granular superconductors that increase the complexity of their study is the presence of grain boundaries **GBs** (see Fig. 1). The **GBs** manifest under different situations and are classified according to the relative misorientation of crystallographic adjacent axes [34]. As displayed in Fig. 2, a distinction between tilt and twist misorientation of the **GBs** is presented. The tilt component is

TABLE I. Critical temperatures and some structural characteristics of the (Bi,Pb)-Sr-Ca-Cu-O superconductors.

Characteristic	Bi- 2201	Bi-2212	Bi-2223
Critical temperature (K)	20	70-90	110
Unit cell type	pseudotetragonal	Idem	Idem
Unit cell dimensions (a=b) ($\dot{A}$)	5.41	Idem	Idem
(c) ($\dot{A}$)	24.6	30.9	37.1
Morphology of the grains	grains with platelet-like shape	Idem	Idem

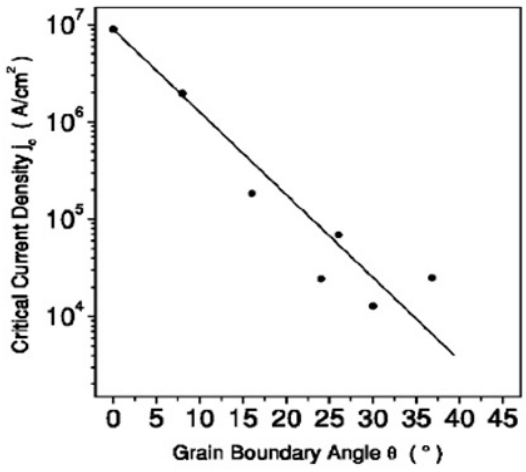

FIGURE 3. Dependence of J_c on misorientation angle, obtained for $T = 26$ K and $B = 0$ T, showing an exponential decay with grain boundary angle. (Figure modified from J. Hänisch *et al.*, [37]).

referred to a rotation around the axis in the plane of the **GB** while the twist one corresponds to a rotation of the crystallite around an axis perpendicular to the **GB** plane. In addition to the **GBs** shown in Fig. 2, other combinations of the tilt and twist components may occur and are termed mixed **GBs**. The **GBs** with identical misorientation components of the grains regarding the intergranular interface are referred as symmetric and in the contrary asymmetric [34].

According to the misorientation angle, θ, of the **GBs**, they are classified as low angle boundaries ($\theta < 10°$) or high angle boundaries ($\theta > 10°$). Following this classification, the low angle boundaries are responsible for the greatest interest for applications [34]. The effects of the **GB** have been studied by several research groups and the literature is rich in the electrical transport properties of thin films, bicrystals and ceramic samples [35–39]. Hänisch and co-authors [37], for instance, have studied the dependence of the current density with the misorientation angle of the **GBs**, θ, in thin films of $Bi_2Sr_2Ca_2Cu_3O_{10+\delta}$. The films were obtained by laser ablation deposition on bicrystalline substrates of $SrTiO_3$ with symmetric **GBs** [001] of $8°, 16°, 24°, 26°, 30°$, and $36.8°$ (see Fig. 3). They observed an exponential dependence of the critical current density of the **GBs** as a function of θ. In addition to this, dissipation by flux creep was detected for $\theta = 8°$ and flux flow for greater angles.

2.2. Superconducting levels

Ji and co-authors [40] have proposed a model in which the granular superconducting material may be described as a system comprised of three superconducting levels: (1) the superconducting grains; (2) the superconducting clusters, or more appropriatelly strongly coupled superconducting grains; and (3) weak links between superconducting clusters. The authors first solved the simplified and special case of infinitely large flat-slab geometry with an ideal ordered superconducting lattice microstructure, where the resulting intergranular fluxon density leads to an anomalous magnetic hysteresis, as experimentally observed. The next step was to generalize this result to disordered samples by introducing a type of clusters of grains. In this case, fluxons move freely in and out of the sample through percolative paths between the clusters, forming a structure topologically identical to the simplified ordered structure. The main obtained result was that the superconducting clusters depend on the microstructure and the stiffness of flux-line lattices, and on whether the sample is cooled in applied magnetic field or not. Finally, the authors used the model to explain features observed in transport critical-current and flux-creep measurements.

2.3. Types of vortices

Three main types of vortices can be identified in the current literature [41] (i) Abrikosov *(A)*; (ii) Josephson *(J)*, and (iii) those described by Gurevich and Cooley [42] which are a mix of the two first and referred to as Abrikosov-Josephson *(AJ)*. The *A* vortices are located in the intragranular region and their cores dimensions is the coherence length, ξ. The

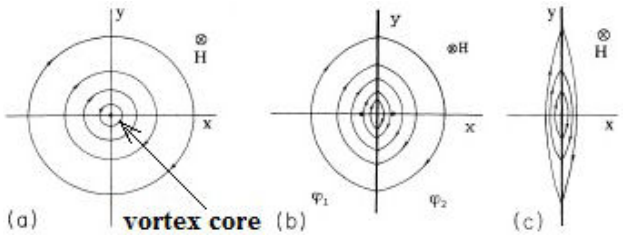

FIGURE 4. Current lines of the different kind of vortices: **(a)**, Abrikosov vortices *(A)*; **(b)**, Abrikosov-Josephson vortices *(AJ)*; **(c)**, Josephson vortices *(J)*. (Figure modified from A. Gurevich [41]).

J vortices appear in the **GBs** regions with high misoorientation angle and low critical current as compared with the intragranular ones. This type of vortices satisfies the condiction $\lambda_J > \lambda$ where λ_J and λ are the Josephson and London penetration depths, respectively. These vortices do not exhibit normal core as the *A* one. Finally, in the case of the *AJ* vortices the condiction to be obeyed is $\lambda_J < \lambda$, and the vortices are mainly located in low misorientation angle **GBs**. In addition to this, for $\theta \sim 2^\circ$, a crossover *AJ-A* is observed [43]. The *AJ* vortices are similar to the *J* vortices because of the absence of a normal core, but they are also similar to the A vortices considering the shape of the current lines in the external region of the vortex (see Fig. 4). Vortices *J* exhibit a weaker pinning when compared to both *A* and *AJ* vortices due to their large dimensions [44].

2.4. Some microstructural characteristics of Bi-Sr-Ca-Cu-O superconductors

After the discovery of the superconductivity in Bi-Sr-Ca-Cu-O [2] system in three phases of the series $Bi_2Sr_2Ca_{n-1}Cu_nO_{2n+4}$ ($n = 1$, 2 and 3), their crystal structures [45–49] and dimensions of the unit cells [50–52] were determined by means of X-rays diffraction patterns of powder samples. The unit cells of the three phases are made up by perovskite blokes of $Sr_2Ca_{n-1}Cu_nO_{1+2n}$ that contain CuO_2 planes parallel oriented to the *ab*-planes. The main difference among the phases is the number of CuO_2 planes which varies from 1 to 3 for the phases 2201, 2212, and 2223 phases, respectively. Thus, the crystal structures of the different phases are made up of CuO_2 planes separated along the *c* direction by calcium layers and SrO and BiO planes [53].

As a general rule, the phases are described as a pseudo-tetragonal unit cell with dimensions $a = b = 5.41\ \dot{A}$ and $c = 24.6\ \dot{A}$ (n = 1), $30.9\ \dot{A}$ ($n = 2$), and $37.1\dot{A}$ ($n = 3$), respectively [53] (see Table I).

In the case of the 2212 and 2223 phases described above, the crystalline structures present a very weak chemical link along the *c* direction [54]. For this reason, polycrystalline specimens of these phases have platelet-like grains which are between 10-100 times greater in their *ab*-planes than along the *c* direction [8]. Another important microstructural feature of this type of granular superconductor is that high-quality grains of the 2223 phase contain stacking fault defects, originating the 2212 phase within the grain. These defects may be detected by measurements of low DC-field microwave absorption **(LFMWA)** and by transmission electron microscopy **(TEM)** [55]. These planar defects may act as intragranular Josephson junctions naturally existing in the crystal structure of Bi-2223 compounds due to the repeated alteration of the nearly insulating atomic planes with the highly conducting CuO_2 atomic planes along the *c*-axis [55]. Recently, we have obtained some high resolution transmission electron microscopy **(HRTEM)** images where such a stacking fault defect has been observed (see Fig. 5). These **(HRTEM)** images were obtained by using a field emission transmission electron microscope, JEM-2200FS, 200 kV, with 0.19 nm resolution in TEM mode. For this purpose, a dry powder sample was dispersed in isopropanol and deposited onto a Formvar carbon copper grid. Notice the scale of both images: they are smaller than the mean size of the grains [56]. In fact, the images further indicate that the grains of the 2223 phase contain planar defects, identified by repeated alteration of the CuO_2 planes along the *c*-axis [55].

Single phase specimens of the 2223 phase are not strighforward obtained. Since the first intents to produce single phase of the 2223 superconducting material, the partial substitution of bismuth by lead [53, 57] showed good results in obtaining superconducting ceramics with high percentage of the 2223 phase, $T_c \sim 105$ K, and a reduction in the sintering temperature from $\sim 900^\circ$C to $\sim 850^\circ$ C. However, only the

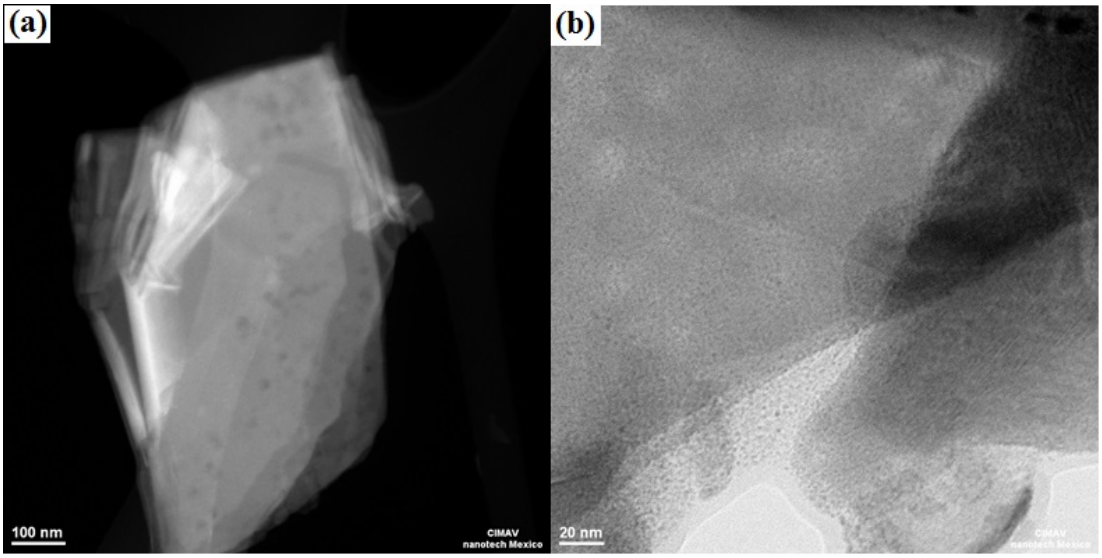

FIGURE 5. High resolution transmission electron microscopy (HRTEM) images of the Bi-2223 powder sample.

TABLE II. Some values of lower critical field, H_{c1}, determined for different type of samples, and directions of applied magnetic field respect to the crystallites axes. The measurement temperature was 77 K in all the cases.

H_{c1}(Oe)	**Type of sample and applied magnetic field direction**	**Reference**
8	tape sample and parallel to the ab-plane	[7]
60	whisker sample and parallel to the c-axis	[6]
25	textured bulk and parallel to the ab-plane	[5]
150	textured bulk and parallel to the c-axis	[5]
80	powder sample and random orientation	[8,9]

partial substitution of bismuth by lead does not guarantee single phase specimens. The phase equilibria in the Bi-Sr-Ca-Cu-O phase diagram is rather complex and displays several different crystal phases at constant pressure and variable temperature. This kind of phase diagram is described elsewhere [54, 57]. Taking into account the complexity of the phase diagram and the high stability of the phase 2212 and the actual occurrence of a Pb-rich extra pahse (Ca_2PbO_4) to obtain a single phase specimen of the (Bi,Pb)-2223 superconductor constitutes a complicate and exhausting task.

A series of works developed by D. Pandey and co-authors [58–62] describe a detailed study on the influence of several variables as the starting lead content, sintering temperature and sintering time for obtaining single pahse 2223 by using the co-precipitation method. Also, the synthesis of (Bi,Pb)-2223 following the traditional ceramic method has been reported [63]. In the previous work Pierre *et al*. reported that the optimal lead concentration is found in the interval $0.3 \leq x \leq 0.4$. Later, P. Muné and co-authors [8] and E. Govea-Alcaide *et al*. [9] obtained almost single phase (Bi,Pb)-2223 samples doped with $x = 0.35$ and 0.36, respectively. In both studies the traditional ceramic method was applied, as described elsewhere [64, 65]. Table I displays some of the main characteristics of the system.

3. Review of experimental and theoretical results

3.1. Magnetic flux penetration

3.1.1. Determining the lower critical field, H_{c1}

In several studies the applied magnetic field dependence of the magnetization, $M(B_a)$, is used for determining the lower critical field, H_{c1}, of a given superconducting material [5,8,9]. When the $M(B_a)$ dependence is obtained in bulk samples (see Fig. 6b), the intergranular value H_{c1} may be estimated. A value of $H_{c1} = 25$ Oe at 77 K, in (Bi,Pb)-2223 ceramic samples was reported elsewhere [55]. On the other hand, such a measurement in powder samples could allow one to estimate the intragranular H_{c1} (see Fig. 7c) [9]. Such an estimate has been performed in two different ways: fitting the curve by means of the Bean model [66] or graphically, where H_{c1} is determined as the field in which the $M(B_a)$

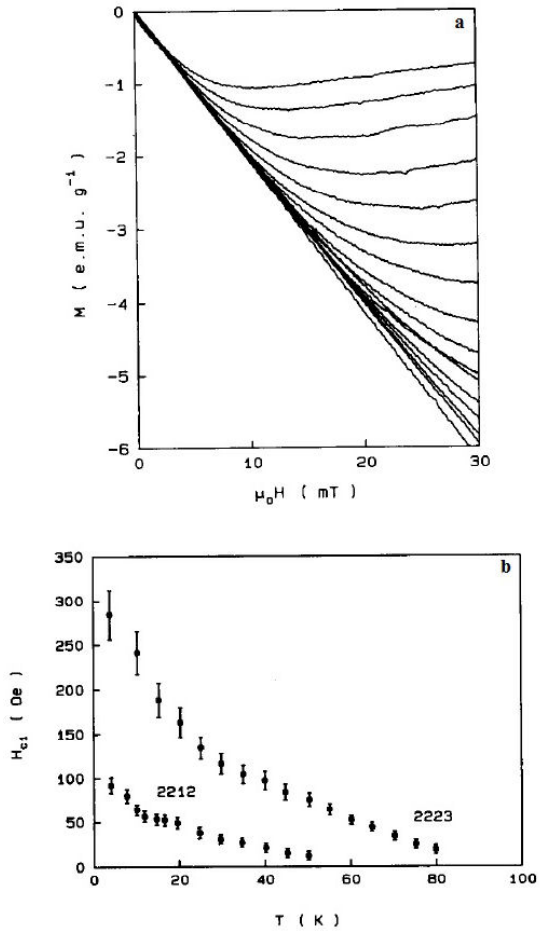

FIGURA 6. **(a)** Virgin magnetization curves of $(Bi, Pb) - 2223$ for temperatures between 4 K (lower curve) and 80 K (upper curve) in steps of about 5 K. H_{c1} can be determined from the deviation from linearity. **(b)** Temperature dependence of the lower critical field H_{c1} for a $(Bi, Pb) - 2223$ and $Bi - 2212$ sample. (Figure modified from R. Job and M. Rosenberg [5]).

curve abandons its quasi-linear behavior. However, a detailed analysis of the quasi-linear region of the $M(B_a)$ curve has yielded a close relationship with the flux-trapping curve [67], measured in bulk sample of (Bi,Pb)-2223 [56,68] (see Fig. 8).

Matsubara *et al.* [6] estimated $H_{c1} = 60$ Oe at 77 K when the magnetic field is applied parallel to the *c*-axis in whiskers of Bi-2223. On the other hand, Majoros *et al*. [7] determined

the intergranular critical field in Bi-2223/Ag tapes, which resulted to be ~ 8 Oe. In this case, the magnetic field was applied perpendicularly to the *c*-axis. These results agree with reference 4 since the values of H_{c1} are approximately related by a factor of 5 or 6 times.

Despite that the lower critical field of the grains, H_{c1g}, at 77 K has been determined in powder samples [8, 9], the experimental results do not reflect the marked anisotropy of the grains. In addition, several different values of H_{c1} can be found in the literature [5–9, 69] (see Table II). In Fig. 9 a hypothetic diagram of the granular structure of these materials is shown. Three types of vortices have been identified. Such a diversity of intergranular vortices could be the cause of the wide spectrum of reported values for the lower critical field in bulk samples. The vortex identified by the number 1 corresponds to the H_{c1} value reported by Matsubara *et al*. [6], since the magnetic field is parallel to the *c*-axis. On the other hand, the vortices 2 and 3 could correspond to the values reported by M. Majoros *et al*. [7] or R. Job and M. Rosenberg [5] because in both cases the magnetic field is parallel to the *ab*-plane (see Table II).

3.1.2. Dependence of the critical current density on increasing applied magnetic field: virgin curve

Several authors have used these curves to characterize the granularity of ceramic superconductors [8, 9]. Figure 7a shows the virgin curves of five (Bi,Pb)-2223 ceramic samples which were obtained under different compacting pressures before the last heat treatment in the synthesis. The intention in subjecting the powders to different uniaxial compacting pressures was to increase the degree of texture throughout the series, further decreasing the granular character of the material [9]. Samples T1 and T2 exhibit an abruptly drop in the critical current density with increasing applied magnetic fields from zero up to 2 mT, where the critical current density has decreased 60 % approximately. It reflects that those samples present a high number of weak links that are penetrated at very low applied magnetic field. This kind of behavior is seen very often in ceramic samples of cuprates and not only in those from the Bi-system. Here, the weak links correspond to high angle **GBs**. Thus, we can assume that the virgin curves exhibit clear evidence of the existence of weak links in these samples. The next step is how one may identify the superconducting clusters by using the flux-trapping curves, as described below.

3.2. Magnetic flux trapping.

3.2.1. Dependence of the critical current density on a maximum applied magnetic field: flux trapping curve

E. Altshuler *et al.* [67] obtained, by the first time, the flux trapping curve, allowing the detection of the trapped flux in a granular sample by using the weak links presented inside the material as sensors. If the sample is submitted to a value of maximum applied magnetic field B_{am} for 30 s and then it is decreased to zero, some magnetic flux will be trapped within the sample. Such a trapped flux may be detected by means of the critical current density measurements of that sample.

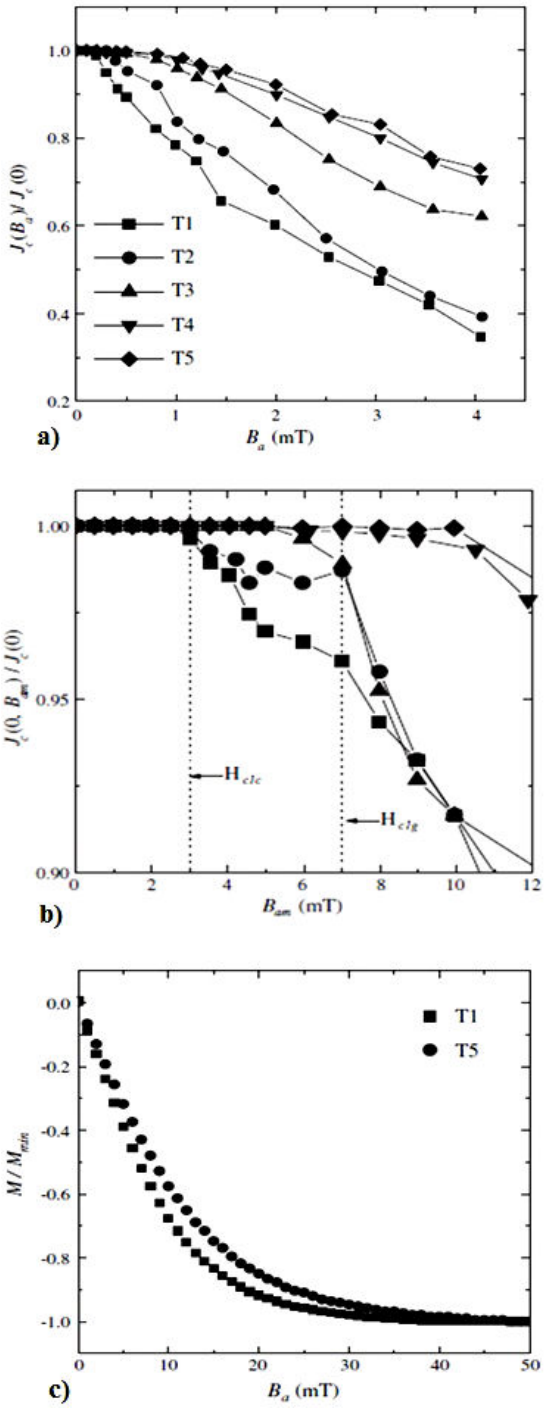

FIGURA 7. Experimental evidences of the three levels of superconductivity: **(a)** Experimental virgin curves, **(b)** Experimental flux-trapping curves y **(c)** Normalized magnetization versus applied magnetic field $M(B_a)$. (Figure modified from E. Govea-Alcaide *et al*., [9]).

Figure 7b shows a group of the flux trapped curves. The normalized critical current density as a function of maximum

applied magnetic field decreases for $B_{am} > 3$ mT in T1 and T2 samples [9]. The main result obtained by E. Govea-Alcaide *et al*. [9] by means of the analysis of the curves displayed in Fig. 7 revealed the presence of three superconducting levels, as described before [40]: the superconducting grains, the superconducting clusters, and the weak links. In addition, the authors found appreciable changes in the distribution of these three superconducting levels with the increase of the compacting pressure used during the elaboration process of the samples. Here, we give a summary of the analysis of those experimental data. The data of Fig. 7a allow to identify the interval of applied magnetic field in which the magnetic flux penetrates the weak links as Josephson vortices [41]: these regions correspond to the high angle **GBs** ($\theta > 10^{\circ}$) which are penetrated for applied magnetic fields ~ 2 mT [8, 9]. On the other hand, Fig. 7c, which was a result of measurements performed in powder samples, allows to determine an approximated value of $\mu_0 H_{c1g}$, that represents the magnetic field of the grains penetration by *A* vortices [41]. Some previous results for Bi-2223 situate this value ~ 8 mT [8, 9] at 77 K. Finally, Fig. 7b displays the intermediate region in terms of applied magnetic field, 3 mT $< B_a <$ 7 mT, corresponding to the magnetic flux trapped by the low angle **GBs** [37, 43], identified as superconducting clusters. However, there are some occult aspects in this explanation because of insufficient experimental verification. Let us formulate them as questions:

1. What are the dimensions of the superconducting clusters? Are they really larger than the physical grains?
2. The $M(B_a)$ curve is not linear for $B_a < 7$ mT [56,68]. How does the linear approximation affect the H_{c1g} determination performed elsewhere [8, 9]?
3. Why is the high anisotropy of the (Bi,Pb)-2223 ceramic superconductors [56, 68] undetectable in these experiments?

In addition to these previous questions, other two may be considered to complete the framework of the three level superconducting system.

1. How do the artificial pinning centers modify the magnetic flux trapping inside the clusters?
2. Could the magnetic flux relaxation of the clusters be observed and characterized?

These questions are close related to the basic assumptions of the three levels model [8,9] used for describing the mechanisms of penetration, trapping, and relaxation of the magnetic flux in Bi-2223 ceramic superconductors. Moreover, Fig. 8 shows clearly the similarity between the magnetic flux penetration process in a powder sample, expressed by the curve dM/dH_a as a function of the applied magnetic field, and the magnetic flux trapping process in a bulk sample given by the flux trapping curve of the same superconducting material. In

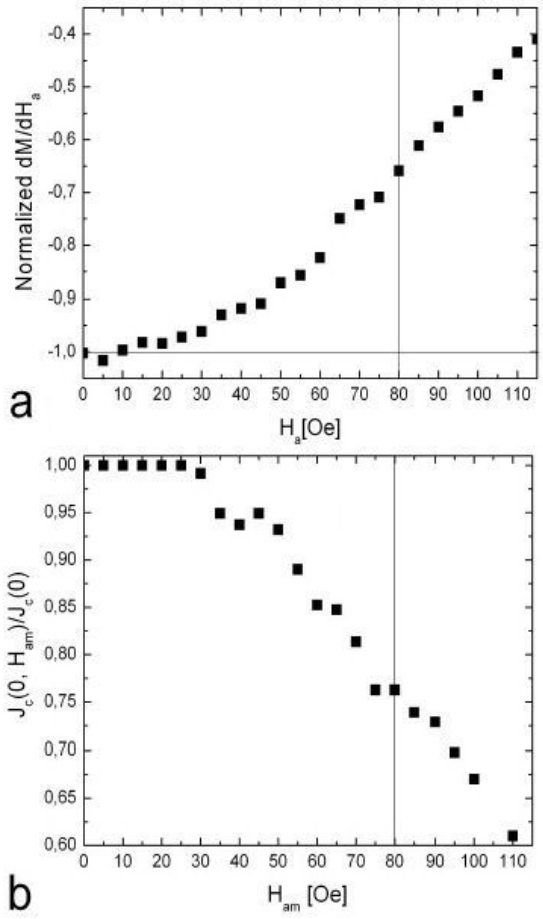

FIGURA 8. **(a)** Normalized dM/dHa as a function of applied magnetic field of the powder sample. For the interval $0 < H_a < 90$ Oe the experimental error does not exceed 5%. **(b)** Flux-trapping curve of the pellet sample. The continuous horizontal and vertical lines visualize the value of normalized dM/dH_a at $H_a = 0$ and the value of the applied magnetic field of 80 Oe, respectively. (Figure reproduced with permission of the RCF and taked from P. Muné *et. al*. [68]).

this case a Bi-2223 sample doped with Ca and Cu was used. Although a small percentage of Bi-2212 phase was detected by means of the X-ray diffraction patterns, its superconducting critical temperature was approximately 70 K, which resulted to be smaller than the measurement temperature that was 77 K. Thus, the magnetic flux could not be trapped by the grains of the low critical temperature phase under those measurement conditions. On the other hand, the similarity between the curves mentioned before suggests that the magnetic flux is trapped within the grains. References 56 and 68 proposed some experiments that could be employed for clarifying the first three points raised above. We will return on these aspects later, at the end of this review.

3.2.2. Alumina nanoparticles addition and its effects on the transport properties

Let us discuss now how the addition of $\alpha-Al_2O_3$ nanoparticles in (Bi,Pb)-2223 matrix [23–25] has been discussed in

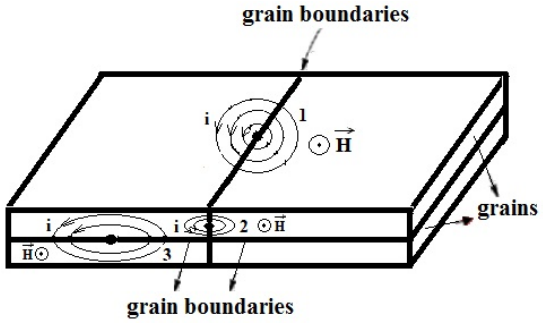

FIGURA 9. Hypothetic schema of some intergranular vortices wich could be related with the different values of H_{c1} reported in Table II.

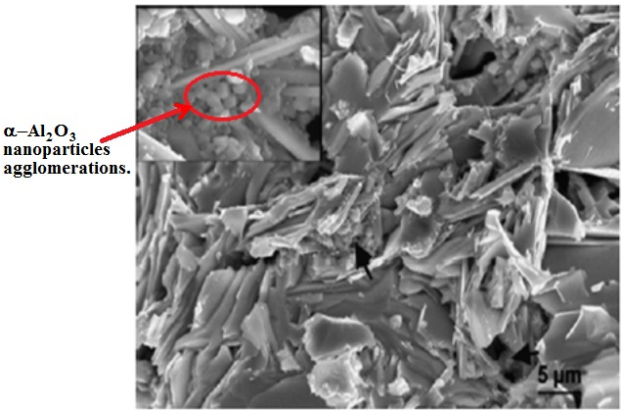

FIGURA 10. SEM micrograph of a transverse cross-section of the 0.5 wt. % $\alpha-Al_2O_3$ doped sample sintered at 830°C for 72 h. Inset: high magnification SEM micrograph. (Figure modified from A. Ghattas *et al*. [24]).

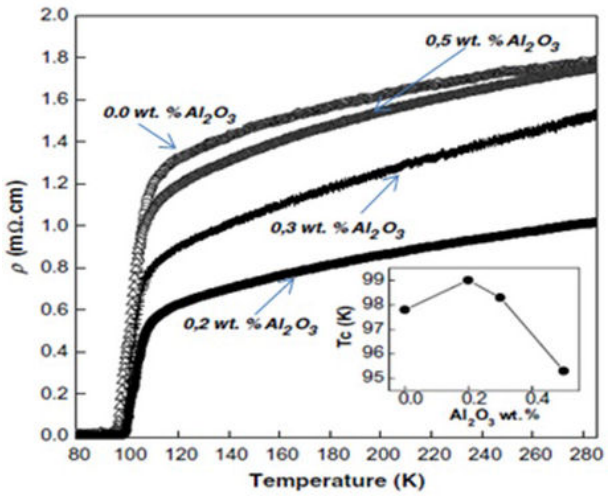

FIGURA 11. Resistivity dependences on the temperature for samples with various amounts of $\alpha-Al_2O_3$ nanoparticles added. Inset: zero-resistivity temperature versus the $\alpha-Al_2O_3$ weight percentage. (Figure modified from A. Ghattas *et al*. [24]).

the literature since the introduction of artificial pinning centers could be an effective tool for studying the superconducting cluster properties and the vortex dynamics in this superconducting level.

M. Annabi *et al*. [23] have studied the addition of nanosized $\alpha-Al_2O_3$ during the final processing of (Bi,Pb)-2223 superconductors. In these experiments the last sintering temperature was also used as a process variable. One of the reults that they obtained was that the sample with 0.2 wt. % of $\alpha-Al_2O_3$ nanoparticles has the higher value of the critical current density $J_c = 160$ A/cm^2, and corresponds to a sample sintered at 835°C.

Another work related to the addtion of $\alpha-Al_2O_3$ nanoparticles in (Bi,Pb)-2223 was developed by A. Ghattas *et al*. [24]. (Bi,Pb)-2223 samples with addition of $\alpha-Al_2O_3$ nanoparticles between 0 and 1 wt.% were synthesized. The authors concluded that, based on Scanning Electron Microscopy (SEM) data, for a doping greater than 0.5 wt. % $\alpha-Al_2O_3$ (see Fig. 10) a heterogeneous distribution of the nanoparticles is observed, which affects the electrical transport properties characterized by measurements of the temperature dependence of the electrical resistivity, $\rho(T)$, as dis-

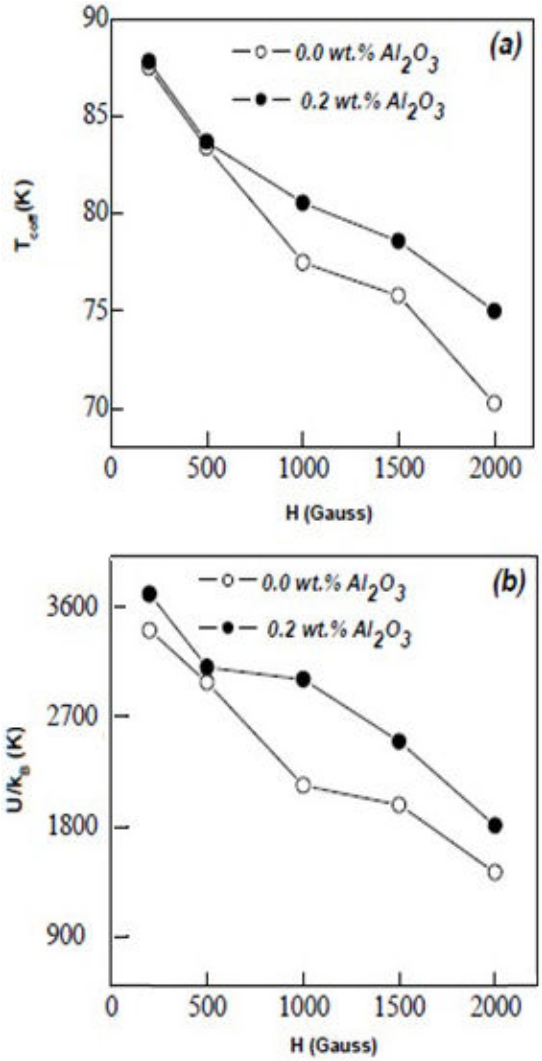

FIGURA 12. T_{coff} **(a)** and effective pinning energy, U, **(b)**, as a function of applied magnetic of free and 0.2 wt. % $\alpha-Al_2O_3$ added samples. In all curves lines between points are guides for eyes. (Figure modified from A. Ghattas *et al*. [25]).

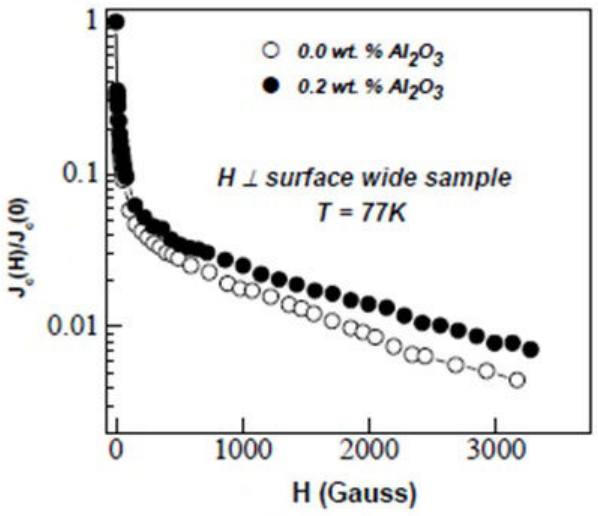

FIGURA 13. Magnetic field dependences of normalized critical current densities obtained with H perpendicular to the surface wide sample at 77 K (Figure modified from A. Ghattas *et al*. [25]).

displayed in Fig. 11. The sample with 0.2 wt. % $\alpha-Al_2O_3$ exhibits the lowest values of the electrical resistivity in the normal state (see the inset). On the other hand, the $\rho(T)$ curve of the sample with 0.5 wt. % $\alpha-Al_2O_3$ is close to the behavior of the sample without addition of nanosized $\alpha-Al_2O_3$ (see Fig. 11). In a third work [25], based on the results of the reference [24], two other samples were studied: a sample without addition of $\alpha-Al_2O_3$ nanoparticles and a second one with 0.2 wt. % $\alpha-Al_2O_3$. Besides the features of the $\rho(T)$ curves, the effective pinning energy as a function of the applied magnetic field, (see Fig. 12) and the dependence of the critical current density on applied magnetic field (see Fig. 13), were obtained. The authors found that the critical temperature of zero resistivity in the doped sample is greater than the one corresponding to sample without addition of $\alpha-Al_2O_3$ nanoparticles. The doped sample also exhibits a better behavior under applied magnetic fields. The intergranular effective pinning energy dependence on the applied magnetic field is greater and the normalized critical current density displays a better behavior for the sample with 0.2 wt. % $\alpha-Al_2O_3$ nanoparticles (see Fig. 12 and Fig. 13), respectively. On the other hand, if we compare the size of vortices's core with the size of nanoparticles, the second are greater and could be hard think that these nanoparticles can became in pinning centers; however the vortices, can not remain trapped at the nanoparticles for the core region, but it could be trapped by a nanoparticle located in the region where the superconducting current of the vortex is circulating [70]. To summarize, the sample with addition of $\alpha-Al_2O_3$ nanoparticles exhibits better superconducting transport properties than the one without addition, but the study was performed under intermediate applied magnetic field $\sim$ 1 T. With this kind of study it is difficult to sense effects of the doping on the behavior of the superconducting clusters.

3.3. Magnetic flux relaxation

After analyzing the penetration and trapping mechanisms of the magnetic flux inside (Bi,Pb)-2223 materials, we now to discuss how the trapped vortices in the superconducting clusters may be affected by the thermal activation. We have selected the case in which the applied magnetic field is zero in order to isolate the type of vortex of our interest. Considering the flux trapping curves, it seems to be that we are in presence of the flux-creep relaxation. The first models for explaining the magnetic relaxation were proposed by Anderson and Kim [71, 72]. Those models were based on the magnetic flux thermal activation in which the pinning centers following a ratio proportional to $\exp(-U/kT)$, where *U* represents the activation energy, *k* is the Boltzmann constant and *T* is the absolute temperature. This process lead to a re-distribution of the vortices and the current lines associated to them causing a change in the magnetic moment of the superconducting sample or level inside the superconducting material. The Anderson-Kim model [71, 72] model predicts that the magnetic moment of the sample varies logarithmically with time, as has been observed elsewhere [73]. According to the Arrhenius relationship, the jump time is given by the following expression:

$$t = t_0 \exp(-U/kT) \tag{1}$$

where the pre-exponential, t_0, is referred to as the time of jump intent, may differ of the microscopic intent time in several orders of magnitude. The jump process is assisted by the force $\vec{F} = (1/c)\vec{J}\times\vec{B}$. Thus, *U* should be a decreasing function of the critical current density *J*. In a first approximation, the barrier energy is reduced to a linear case with *J*

$$U = U_0\,[1 - J/J_{c0}] \tag{2}$$

where $J_{c0} = cU_0/Bx_0V$ is the current critical density at which the barrier is suppressed. Here, c, U_0, x_0, B, and V are the light speed, the barrier energy, the jump distance, the applied magnetic field, and the volume of the flux bundle, respectively. Several modifications have also been introduced to the expression (2) [44, 74, 75] in order to describe in a better way the phenomena observed in **HTS**.

As described in Sec. 1, several authors have reported magnetic relaxation by transport measurement [27–29] but no relaxation was observed when the maximum applied magnetic field at which the sample was submitted was lower than H_{c1g}. Let us then describe briefly how those measurements were performed. When a transport current is conveniently applied to a superconducting granular sample, which was submitted to a process of trapping flux as described previously, the dissipation voltage decreases as a function of time according to the following expression, [28]:

$$V(t) = V(0)\,\{1 - [kT/U]\,ln\,(1 + t/t_0)\} \tag{3}$$

where $V(0)$ is the voltage in $t = 0$ and the remaining parameters were already defined above. There are several studies where the magnetic relaxation of granular superconductors

are reported. However, intergranular relaxation in superconducting clusters has not been reported as far as we know. A combining study by means of flux-trapping curves, voltage relaxation, and magnetization relaxation in bulk and powder samples could help in a deeper understating of the three superconducting levels model [40].

4. Conclusions

(Bi,Pb)-2223 ceramic samples obtained at low compacting pressures evidence the existence of three superconducting levels, as inferred by transport and magnetic measurements. However, other experiments can be still performed in order to go deeper in the understanding of systems comprised of the three levels, as granular superconducting cuprates. Here, we summarize some of them:

1. Although in references [8, 9] the authors claim the presence of superconducting clusters as grains strongly linked, some current experimental results demonstrate that the flux penetration in a powder sample observed by $M(B_a)$ measurements is closely related to the flux-trapping curve [67] in a bulk one of the same superconducting material. Thus, the effects of the flux penetration inside superconducting clusters are also observed in powder samples [56, 68].

2. A detailed study of the superconducting grain structure is also necessary. Usually, the superconducting grains are considered as single crystals as a first approximation. However, the presence of defects inside the grains in a very complex structure obtained by ceramic method is obviously expected. The causes of the experimental results described in the first conclusion could be found for this via.

3. Measurements of the flux-trapping curves in bulk or magnetization versus applied magnetic field in powder samples at different temperature would allow determining the temperature dependence of the penetration field for both superconducting clusters and superconducting grains, and also evaluating the nature of the magnetic flux located within the clusters.

4. The addition of α-Al_2O_3 nanoparticles in samples obtained at low compacting pressure would allow studying the effects of this addition on the penetration, trapping and relaxation of the vortices trapped in superconducting clusters which are expected to be AJ vortices located in low-angle GBs.

5. As the high anisotropy of the (Bi,Pb)-2223 is not reveled in the $M(B_a)$ curves of powder samples at 77 K, it could reinforce the idea that the powder grains do not behave as single crystals at least at this temperature.

All the aspects enumerated on the subject have not been discussed partially or totally in the literature, as far as the authors know.

Acknowledgments

This work was partially financed by the Brazil's agency Fundação Coordenação de Aperfeiçoamento de Pessoal de Nível Superior (CAPES) under Grant No. 104/10 and FAPESP under Grant No. 2013/07296-2 and 2014/19245-6. One of the authors, M. Hernández-Wolpez, was supported by the Agreement of Collaboration between Universidad de Camagüey, Cuba, and Facultad de Ciencias Físico-Matemáticas de la Universidad Autónoma de Nuevo León, Monterrey, México. We would like to express our gratitude to M.C. César Cutberto Leyva Porras for the HRTEM images of (Bi,Pb)-2223 powder samples.

1. J.G. Bednorz and K.A. Müller, *Z. Phys. B* **64** (1986) 189.
2. H. Maeda, Y. Tanaka, M. Fukutomi and T. Asano, *Jpn. J. Appl. Phys.* **27** (1988) L209.
3. D. Larbalestier, A. Gurevich, D. Matthew Feldmann and A. Polyanskii, *Nature* **414** (2001) 368.
4. H. Adrian, W. Assmus, A. Hohr, J. Kowalewski, H. Spille and F. Steglich, *Physica C* **162-164** (1989) 329.
5. R. Job and M. Rosenberg, *Physica C* **172** (1991) 391.
6. I. Matsubara, R. Funahashi, K. Ueno, H. Yamashita, and T. Kawai, *Physica C* **256** (1996) 33.
7. M. Majoros, L. Martini and S. Zannella, *Physica C* **282-287** (1997) 2205.
8. P. Muné, E. Govea-Alcaide and R. F. Jardim, *Physica C* **384** (2003) 491.
9. E. Govea-Alcaide, R.F. Jardim and P. Muné, *Physica C* **423** (2005) 152.
10. T.P. Orlando and K.A. Delin, *Foundations of Applied Superconductivity.* (Adisson- Wesley, New York. 1991).
11. A. Díaz, J. Maza and F. Vidal, *Phys. Rev. B* **55** (1997) 1209.
12. H.W. Neumuller, W. Gerhauser, G. Ries, P. Kummeth, W. Schmidt, S. Klaumunzer and G. Saemann-lschenko, *Cryogenics* **33** (1993) 14.
13. A. K. Pradhan *et al*., *Phys. Rev. B* **55** (1997) 11129.
14. R. Gerbaldo *et al*., *Materials Science and Engineering B* **55** (1998) 109.
15. E. Mezzetti *et al*., *IEEE Transactions on Applied Superconductivity* **9** (1999) 1872.
16. P. Sen, S.K. Bandyopadhyay, P.M.G. Nambissan, P. Barat and P. Mukherjee, *Phys. Lett. A* **302** (2002) 330.

17. D. Botta *et al*., *Physica C* **408-410** (2004) 32.
18. I.A. Rudnev, B.P. Mikhailov and P.V. Bobin, *Tech. Phys. Lett. Vol.* **31** (2005) 176.
19. A.V. Pop, R. Deltour, A. Harabor, D. Ciurchea, Gh. Ilonca, V. Pop and M. Todica, *Supercond. Sci. Technol.* **10** (1997) 843.
20. M.S.A. Hossain, J.H. Kim, X. Xu, X.L. Wang and S.X. Dou, *J. Phys. Conference Series* **97** (2008) 012066.
21. A.I. Abou-Aly, S.A. Mahmoud, R. Awad and M.M.E. Barakat, *J. Supercond. Nov. Magn.* **23** (2010) 1575.
22. D. Yazici, M. Erdem and B. Ozcelik, *J. Supercond. Nov. Magn.* (2011).
23. M. Annabi, A.M. Chirgui, F. Ben Azzouz, M. Zouaoui and M. Ben Salem, *Physica C* **405** (2004).
24. A. Ghattas, M. Annabi, M. Zouaoui, F. Ben Azzouz, and M. Ben Salem, *Physica C* **468** (2008) 31.
25. A. Ghattas, F. Ben Azzouz, M. Annabi, M. Zouaoui and M. Ben Salem, *J. Phys. Conference Series* **97** (2008) 012175.
26. Y. Yeshurun, A.P. Malozemoff and A. Shaulov, *Rev. Mod. Phys.* **68** (1996) 911.
27. E. Altshuler and J.L. González, *Physica C* **200** (1992) 195.
28. D.N. Matthews, G.J. Rusell and K.N. R. Taylor, *Physica C* **171** (1990); see also D.N. Matthews, G.J. Rusell, K.N.R. Taylor and G. Álvarez. in: Proc. ICTPS 90 Int. Conf. on Transport Properties of Superconductors, Rio de Janeiro, April 29-May 4, (1990).
29. R. Decca, E. Altshuler and L. Fábrega, *Workshop in High Tc Superconductors and Related Materials* (Advanced Activities). ICTP, Trieste, Nov.-Dec. (International Report), (1990).
30. J.R. Clem, *Physica C* **153-155** (1988) 50.
31. S. Graser, P.J. Hirschfeld, T. Kopp, R. Gutser, B.M. Andersen and J. Mannhart, *Nat.* **6** (2010) 609.
32. M.R. Cimberle *et al*., *Physica C* **251** (1995) 61.
33. D. Daghero, A. Masuero, P. Mazzetti and A. Stepanescu, *Physica C* **341-348** (2000) 1869.
34. H. Hilgenkamp and J. Mannhart, *Rev. Mod. Phys.* **74** (2002) 485.
35. D. Dimos, P. Chaudhari, J. Mannhart and F.K. LeGoues, *Phys. Rev. Lett.* **61** (1988) 219.
36. D. Dimos, P. Chaudhari, and J. Mannhart, *Phys. Rev. B* **41** (1990) 4038.
37. J. Hänisch, A. Attenberger, B. Holzapfel and L. Schultz, *Phys. Rev. B* **65** (2002) 052507.
38. R. Held *et al*., *Phys. Rev. B* **79** (2009) 014515.
39. I. García-Fornaris. Tesis de Doctorado. Universidad de La Habana, Cuba, (2011).
40. L. Ji, M.S. Rzchowski, N. Anand and M. Tinkham, *Phys. Rev. B* **47** (1993) 470.
41. A. Gurevich, *Phys. Rev. B* **48** (1993) 12857.
42. A. Gurevich and L.D. Cooley, *Phys. Rev. B* **50** (1994) 13563.
43. M. Mora, Tesis de Doctorado, Universidad de Zaragoza, España, (1998).
44. G. Blatter, M.V. Feigelman, V.B. Geshkenbein, A.I. Larkin and V.M. Vinokur, *Rev. Mod. Phys.* **66** (1994) 1125.
45. H.G. von Schneering *et al*., *Angew. Chem* **27** (1988) 574.
46. J.L. Tallon *et al*., *Nature* **333** (1988) 153.
47. P. Bordet *et al*., *Physica C* **153-155** (1988) 623.
48. B.W. Statt *et al*., *Physica C* **157** (1988) 251.
49. D. Shi, M. Tang, K. Vandervoort and H. Claus, *Phys. Rev. B* **39** (1988) 9091.
50. D. Pandey, R. Mahesh, A.K. Singh, V. S. Tiwari and S.K. Kak, *Physica C* **184** (1991) 135.
51. E. Giannini, I. Savysyuk, V. Garnier, R. Passerini, P. Toulemonde and R. Flukiger, *Supercond. Sci. Tech.* **15** (2002) 1577.
52. V.F. Shamray, A.B. Mikhailova and A.V. Mitin, *Cryst. Rep.* **54** (2009) 584.
53. J.-C Grivel, R.E. Gladyshevskii, E. Walter, R. Flukiger, *Physica C* **274** (1997) 66.
54. P. Majewski, *J. Mater. Res*. **15** (2000) 854.
55. V. Kataev, N. Knauf, B. Buchner and D. Wohlleben, *Physica C* **184**, (1991) 165-171.
56. M. Hernández-Wolpez, A. Cruz-García, O. Vázquez-Robaina, R.F. Jardim and P. Muné, *Physica C* **525-526** (2016) 84.
57. W. Wong-Ng, L. P. Cook, A. Kearsley and W. Greenwood, *J. Res. Natl. Inst. Stand. Technol*. **104** (1999) 277.
58. D. Pandey, A.K. Singh, R. Mahesh V.S. Tiwari and S.K. Kak, *Physica C* **173** (1991) 476.
59. D. Pandey, R. Mahesh, A.K. Singh, V. S. Tiwari and S.K. Kak, *Physica C* **184** (1991) 135.
60. D. Pandey, A.K. Singh and A.P. Singh, *Physica C* **204** (1992) 179.
61. D. Pandey, A.K. Singh, P.K. Srivastava, A.P. Singh, S.S.R. Inbanathan and G. Singh. *Physica C* **241** (1995) 279.
62. D. Pandey, S.S.R. Inbanathan, P.K. Srivastava, A. Banerjee and G. Singh, *Physica C* **261** (1996) 157.
63. L. Pierre *et al*., *J. Appl. Phys.* **68** (1990) 2296.
64. V.E. Gasumyants, S.A. Kazmin, V.I. Kaidanov, S.A. Lycov, V.A. Polyakov and S.E. Khabavov, *Sov. Supercond.* **4** (1991) 504.
65. E. Govea-Alcaide, Tesis de Doctorado, Universidad de La Habana, Cuba, (2005).
66. C.P. Bean, *Rev. Mod. Phys.* **36** (1964) 31.
67. E. Altshuler, S. García and J. Barroso. *Physica C* **177** (1991) 61.
68. P. Muné, M. Hernández-Wolpez, A. Cruz-García and R.F. Jardim, *Rev. Cub. Física* **32** (2015) 53.
69. R.B. van Dover, L.F. Schneemeyer, E. M. Gyorgy and J.V. Waszczak, *Phys. Rev. B* **39** (1989) 4800.
70. A. Gurevich, *Supercond. Sci. Technol* **20** (2007) S128.
71. P.W. Anderson, *Phys. Rev. Lett.* **9** (1962) 309.
72. P.W. Anderson and Y.B. Kim, *Rev. Mod. Phys.* **36** (1964) 39.
73. Y.B. Kim, C.F. Hempstead and A.R. Strand, *Phys. Rev. Lett.* **9** (1962) 306.
74. M.V. Feigelman, V.B. Geshkenbein, and V.M. Vinokur, *Phys. Rev. B* **43** (1991) 6263.
75. V.M. Vinokur, M.V. Feigelman and V.B. Geshkenbein, *Phys. Rev. Lett*. **67** (1991) 915.